

## NANOMECHANICAL PROPERTIES AND DRY SLIDING WEAR BEHAVIOR OF CONVENTIONAL AND NANOSTRUCTURED WC-CoCr COATINGS PREPARED BY HVOF SPRAYING

S. HONG<sup>a\*</sup>, Y.P. WU<sup>a</sup>, B. WANG<sup>a</sup>, J.F. ZHANG<sup>a</sup>, Y. ZHENG<sup>b</sup>, L. QIAO<sup>a</sup>

<sup>a</sup>*Institute of Metals and Protection, College of Mechanics and Materials, Hohai University, 8 Focheng West Road, Nanjing 211100, PR China*

<sup>b</sup>*National Engineering Research Center of Water Resources Efficient Utilization and Engineering Safety, Hohai University, 1 Xikang Road, Nanjing 210098, PR China*

The high-velocity oxygen-fuel (HVOF) spraying process was used to fabricate conventional and nanostructured WC-CoCr cermet coatings. The nanomechanical properties and the sliding wear resistance of both coatings were investigated using a nanoindenter and a pin-on-disk high-temperature tribometer, respectively. The results showed that nanostructured coating exhibited slightly lower hardness ( $H$ ), lower elastic modulus ( $E$ ), but slightly higher ratios of  $H/E$  and  $H^3/E^2$ , than conventional coating. The sliding wear resistance of nanostructured coating was about 1.2 times that of conventional coating at 350 °C by the values of wear rate. This was attributed to relatively higher  $H/E$  and considerable amounts of oxide films on the worn surface of nanostructured coating. Main wear modes of conventional coating included carbide particle pull-out following the crack propagation and fatigue delamination, while binder extrusion was the predominant sliding wear mechanism for nanostructured coating in air at 350 °C.

(Received August 25, 2016; Accepted October 27, 2016)

*Keywords:* High-velocity oxygen-fuel; WC-CoCr; Nanostructured; Nanomechanical; Wear

### 1. Introduction

Many machine components fitted in aircraft engines, transportation, oil/gas exploration and chemical processing equipment face severe wear damage, which does not only shorten the lifetime of components but also affect the reliability and economy of manufacturing processes [1]. To overcome this problem, great attentions have been paid to the selection of appropriate surface coatings, including nickel-based alloy [2], alumina [3], chromium carbide-based [4,5], tungsten carbide-based [6-8], iron-based amorphous [9], and iron aluminide [10,11]. It is evident from literature that tungsten carbide-based cermet coatings have played an important role in reduction of sliding, abrasive and erosive wear damage due to the combination of high hardness and adequate toughness [12-14]. High-velocity oxygen-fuel (HVOF) spraying has been proved to be a more promising technology for deposition of tungsten carbide-based materials compared to other thermal spray processes, which was due to comparatively less decomposition of WC phase as a result of higher flame velocity, lower flame temperature and dwell time [15].

In the case of HVOF sprayed WC-based cermet coating, it has been reported that the sliding wear resistance was related to hardness, toughness, carbide to binder ratio, carbide grain size and carbide-binder interfacial strength. According to most investigators, decreasing the WC grain size from the micron scale to the nanometer scale was beneficial for the hardness, mechanical strength and sliding wear resistance of the coatings [7,13,16-18]. On the contrary,

---

\* Corresponding author: hongsheng1988@126.com

other researchers have reported that conventional WC-based cermet coatings were superior in sliding wear resistance compared to nanostructured ones, which was attributed to more serious WC particles decomposition of nanostructured coatings during spraying [6,19,20]. In addition, the test conditions (e.g. applied load, temperature and atmosphere) also affected the sliding wear resistance and failure mechanism of WC-based cermet coatings. Recently, Wesmann and Espallargas [21] investigated the effect of atmosphere, temperature and carbide size on the sliding friction of HVOF sprayed WC-CoCr coatings. They found that the two main parameters affecting friction and wear were temperature and atmosphere, while the effect of primary carbide size on friction and wear was marginal. Geng et al. [22] pointed out that HVOF sprayed WC-Co coatings should not be used as wear-resistant coatings in O-deficient environments at room temperature or at elevated temperatures. It is noteworthy that although a series of WC-based cermet coatings prepared by HVOF spraying process have been recently investigated, few researches have done to discuss how the nanomechanical properties affect the sliding wear resistance of the nanostructured WC-CoCr coating at elevated temperature. In particular, the wear resistance depended not only on hardness ( $H$ ) and fracture toughness, but also on the reciprocal of elastic modulus ( $E^{-1}$ ). Parameters of  $H/E$  and  $H^3/E^2$  were both vital to evaluate the wear resistance of materials [23-25]. More investigations should be further carried out to relate the nanomechanical parameters to the sliding wear behavior.

Previously, the present authors investigated the effect of spray parameters on the microstructure and sliding wear behavior of HVOF sprayed nanostructured WC-CoCr coatings, and obtained the optimal spray parameter [26]. Conventional and nanostructured WC-CoCr coatings were both synthesized successfully by HVOF spraying process and their microstructures and sliding wear behavior at room temperature were reported [26-29]. This work is an extension of the reported research. The aim of this study was to assess the correlation between the nanomechanical properties and the sliding wear resistance of HVOF sprayed conventional and nanostructured WC-CoCr coatings at elevated temperature.

## 2. Experimental procedure

Commercially available conventional (Large Solar Thermal Spraying Material Co. Ltd, Chengdu, China) and nanostructured (Infralloy-7410, Inframat Advanced Materials Corp., Farmington, CT, USA) WC-CoCr powders with the nominal composition of 4 wt.% Cr-10 wt.% Co-5.3 wt.% C-80.7 wt.% W were used in the present study and their particle sizes were 15~45  $\mu\text{m}$  and 5~45  $\mu\text{m}$ , respectively. The nanostructured powder was agglomerated by fine particles (100~500 nm). These powders were deposited on the AISI 1045 steel substrate by using commercial HVOF thermal spray system (Praxair Tafa-JP8000, USA). Details of HVOF spraying process parameters were given in Table 1. Prior to coating deposition, the substrate samples were pre-cleaned in acetone, dried in hot air, and then grit blasted with 30 mesh  $\text{Al}_2\text{O}_3$  to provide a fresh and rough surface for better adhesion. Then, the substrate samples were cooled with compressed air jets during and after spraying.

Table 1 Process parameters employed for HVOF spray process.

| Spray parameters                                      | WC-CoCr coatings |                |
|---|------------------|----------------|
|   | Conventional     | Nanostructured |
| Oxygen flow rate, $\text{L}\cdot\text{min}^{-1}$      | 897              | 944            |
| Kerosene flow rate, $\text{L}\cdot\text{min}^{-1}$    | 0.38             | 0.38           |
| Carrier gas flow rate, $\text{L}\cdot\text{min}^{-1}$ | 10.86            | 10.86          |
| Spray distance, mm                                    | 300              | 330            |
| Powder feed rate, $\text{g}\cdot\text{min}^{-1}$      | 50               | 50             |
| Spray gun speed, $\text{mm}\cdot\text{s}^{-1}$        | 280              | 280            |

Microstructures of both coatings were observed by a scanning electron microscope (SEM, Hitachi S-3400N, Japan). Porosity measurements were determined by an optical microscopy (OM, Olympus BX51M, Japan) fitted with an image analyzer, on polished cross sections of the coating at a magnification of 500. The nanomechanical properties of both coatings were tested by nanoindentation performed on a Nanoindenter (Agilent G200, USA) with a Berkovich tip. Prior to nanoindentation, top surfaces of the specimens were ground and polished to mirror-like appearance using diamond paste. The loading rate divided by the load was controlled as a constant of  $0.05 \text{ s}^{-1}$  during the tests to maintain a constant indentation strain rate. The maximum indentation depth was 600 nm. The hardness and elastic modulus were obtained from the load-displacement curves using the Oliver-Pharr method [30]. At least 20 indentations for each specimen were performed to verify the accuracy of the indentation data.

The friction and wear tests were carried out on a pin-on-disk high-temperature tribometer (Beilun MG-2000, China) according to standard ASTM G99-05 [31]. Prior to the test, specimens were prepared by sequential grinding with 240-2000 mesh grade SiC abrasive papers, polished by 2.5 and 0.5  $\mu\text{m}$  diamond pastes, then degreased in acetone in an ultrasonic bath and dried in warm air. In the test, the upper pin of  $\text{Al}_2\text{O}_3$  ball ( $\Phi$  6 mm) was stationary, while the counterface disk ( $\Phi$  45 mm  $\times$  7 mm) was rotated. Mating materials were HVOF sprayed conventional and nanostructured WC-CoCr coatings. Each test was performed under the following condition: sliding velocity of  $0.9 \text{ m}\cdot\text{s}^{-1}$  for 30 min, furnace temperature of  $350 \text{ }^\circ\text{C}$  and normal load of 50 N without lubrication. The relative humidity varied between 35 and 55 %. The frictional moments were recorded by a computer consistently. After wear test, the surface roughness ( $R_a$ ) values and the wear tracks of both worn coatings were measured by a profile and roughness tester (Taiming JB-4C, China). The wear rate was calculated by dividing the volume loss by load and sliding distance. The worn surfaces of both coatings were characterized by SEM with an energy dispersive spectroscopy (EDS, EX250). Each test was repeated at least thrice to make sure a good repeatability of the experiment result.

### 3. Results and discussion

#### 3.1 Microstructural analysis of the coatings

Our previous studies [27,28] have shown that conventional and nanostructured WC-CoCr coatings were both successfully prepared by HVOF spraying technology and composed of WC,  $\text{W}_2\text{C}$  and a mixture of amorphous and nanocluster phase. Fig. 1 shows typical regions from the cross-sections of the coatings. It can be noted from Fig. 1(a) and (c) that the thickness of conventional and nanostructured WC-CoCr coatings are about 180  $\mu\text{m}$  and 210  $\mu\text{m}$ , respectively. Both coatings adhere well to the substrates and present homogenous and dense structures without internal cracking that due to high thermal stresses. Comparison of conventional coating observed in Fig. 1(b) with nanostructured coating shown in Fig. 1(d) indicates that nanostructured coating possesses relatively high porosity, although the porosity percentages of both coatings were less than 1 % by the image analysis. In general, the semi-molten droplet containing fine solid WC particles embedded in the molten matrix flows and flattens better than one containing larger WC particles in a molten matrix [32]. However, the shorter spray distance of conventional coating in this study would ensure powder particles have higher temperature and velocity toward the substrate and as-sprayed coatings possess higher density, lower volume fraction of unmelted particles and oxidation products [33,34]. In addition, fine tungsten carbides are well preserved and uniformly distributed in both coatings.

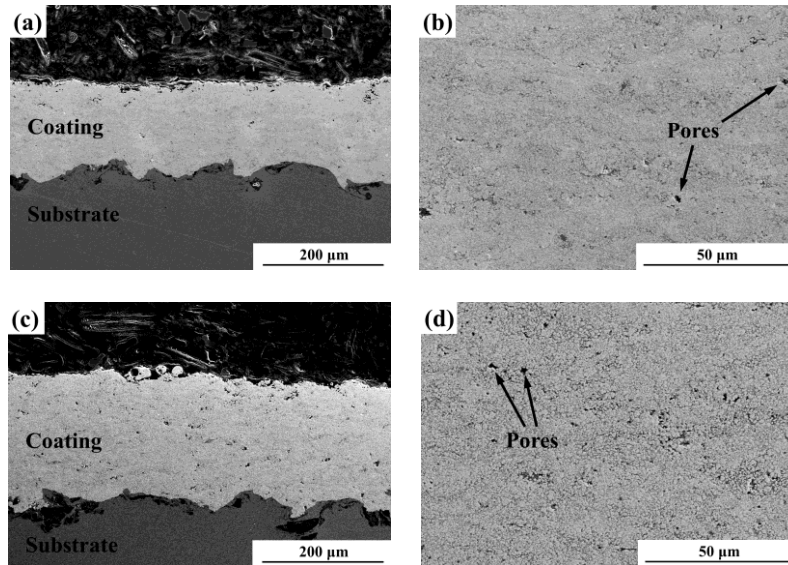


Fig. 1 SEM images of a transverse section of HVOF sprayed conventional (a,b) and nanostructured (c,d) WC-CoCr coatings: (a,c) overall view morphologies; (b,d) pores

### 3.2 Nanomechanical and tribological properties of the coatings

Nanoindentation is a suitable technique to evaluate the mechanical properties of brittle materials [35]. To avoid the influence of the substrate during nanoindentation measurements, less than 10 % of thickness of the coatings was intended. Fig. 2 presents typical load-displacement curves of the coatings, which indicates the presence of an elastic-plastic deformation process as expected for brittle materials. It is clear that the loading-unloading curves of both coatings are smooth. This can be attributed to the low porosity ( $\leq 1\%$ ) and few microcracks throughout the coatings. As compared with nanostructured coating at the same load, conventional coating presents a lower penetration depth, which means that conventional coating possesses relatively high hardness. Decrease in the penetration depth of the indenter is related to the growth of compressive residual stress resulting from the higher impact velocity of spray particles against the substrate surface during the powder deposition process for conventional coating [36]. Table 2 summarizes the measured hardness ( $H$ ) and elastic modulus ( $E$ ) for the coatings. The hardness and elastic modulus of conventional coating are calculated as 26.1 GPa and 468 GPa, respectively. Similar values obtained for nanostructured coating are 24.4 GPa and 414 GPa that are slightly lower when compared to that of conventional coating, which is consistent with the result of load-displacement curves. Besides hardness and elastic modulus, the ratios of  $H/E$  and  $H^3/E^2$  are also important to predict the service life.  $H/E$  is indicative of the depth of penetration which a material can tolerate without exceeding its elastic limit, while  $H^3/E^2$  gives an indication of the resistance of the material to plastic deformation in loaded contact [37,38]. The experimental results reveal that the ratios of  $H/E$  and  $H^3/E^2$  for nanostructured coating are both higher than that of conventional coating. Hence, it can be deduced that nanostructured coating behaves less plastically than conventional coating.

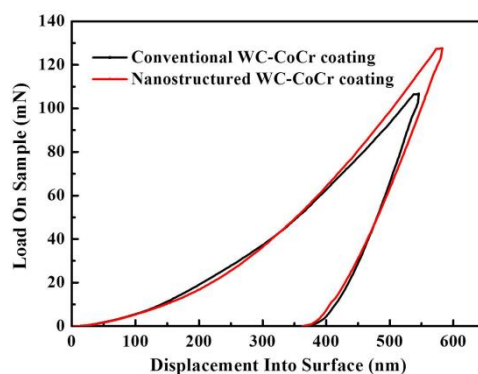


Fig. 2 Load-displacement curves of HVOF sprayed conventional and nanostructured WC-CoCr coatings

Table 2 Nanomechanical properties of the WC-CoCr coatings.

| WC-CoCr coatings | Hardness ( $H$ ),<br>GPa | Elastic modulus ( $E$ ), GPa | $H/E$ | $H^3/E^2$ , GPa |
|------------------|--------------------------|------------------------------|-------|-----------------|
| Conventional     | 26.1                     | 468                          | 0.056 | 0.0812          |
| Nanostructured   | 24.4                     | 414                          | 0.059 | 0.0848          |

Fig. 3 reveals the variation of the friction coefficients with the sliding time for the coatings. In air at 350 °C, the friction coefficient curves of both coatings proceed in a similar trend, consisting of running-in period and steady-state period. The friction coefficient increased quickly during the first few minutes, followed by a slight decrease, and then gradually became stable. It is evident that nanostructured coating exhibit a lower friction coefficient with smaller fluctuation during the steady-state period as compared to that of conventional coating. The initial sharp increase in the friction coefficient may be associated with the high local contact pressures between the coatings and the alumina counterparts, whereas the decrease before steady-state period can be attributed to the enlarged real contact area and the formation of oxide films with lubricating properties [7,16]. To better understand the wear behavior of the coatings, the average friction coefficient during the steady period and the average surface roughness ( $R_a$ ) values of worn surfaces, as well as the wear rate are listed in Table 3. Obviously, nanostructured coating possesses lower friction coefficient,  $R_a$  value of worn surface and wear rate than conventional coating. A simple comparison of wear rate indicates that the wear resistance of nanostructured coating is about 1.2 times that of conventional coating at 350 °C. This may be justified by the larger amounts of the oxide films for nanostructured coating, which is verified by the SEM images of worn surfaces as shown in Fig. 4. A similar result has also been observed by other researchers [39]. In addition, nanostructured coating with relatively higher  $H/E$  could elastically recover the deformation and decrease the number of asperities on the wear surface when external stress above its elastic limit, leading to the decrease in the friction on the sliding contact [35], and then the increase in the wear resistance. It may suggest that the  $H/E$  value is an important parameter in determining the wear resistance of the coatings.

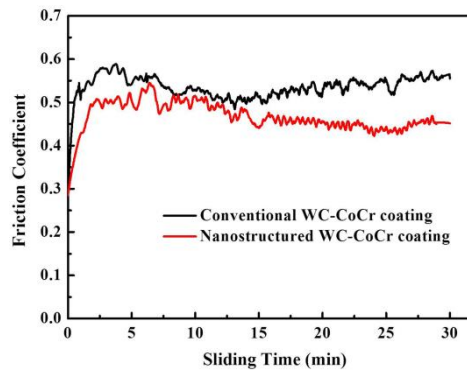


Fig. 3 Friction coefficients varied with sliding time for HVOF sprayed conventional and nanostructured WC-CoCr coatings (counterface  $Al_2O_3$ , load 50 N, temperature 350 °C, sliding velocity  $0.9\text{ m}\cdot\text{s}^{-1}$ ).

Table 3 Summary of friction and wear results for the WC-CoCr coatings.

| Characteristic parameters  | WC-CoCr coatings |                |
|--|------------------|----------------|
|  | Conventional     | Nanostructured |
| Average friction coefficient during the steady period                      | 0.53             | 0.47           |
| Average surface roughness ( $R_a$ ) values of worn surfaces, $\mu\text{m}$ | 0.23             | 0.14           |
| Wear rate, $10^{-5}\text{ mm}^3\cdot\text{N}^{-1}\cdot\text{m}^{-1}$       | 8.36             | 7.25           |

Fig. 4 shows representative SEM images and EDS analyses from worn surfaces of the coatings against  $Al_2O_3$  ball at 350 °C under a load of 50 N. After sliding for 30 min, the worn surface of nanostructured coating (Fig. 4(d)) with more coverage of dark grey materials is smoother than that of conventional coating (Fig. 4(a)), which is consistent with the  $R_a$  values of worn surfaces as listed in Table 3. The friction coefficients in Fig. 3 also show that nanostructured coating is more stable as compared to that of conventional coating may mainly due to its smoother surface. The EDS spectrum of point A (Fig. 4(c)) and point B (Fig. 4(f)) reveals that the regions in dark grey tone contain primarily Co, W and O indicating the presence of mixed W and Co oxides. The quantitative analysis (wt.%) of these points is also given in Fig. 4(c) and (f), respectively. Interestingly, the oxidized clusters are found on the worn surfaces of both coatings, although they are more numerous in a widespread dispersion for nanostructured coating. This may be associated with the relatively homogeneous microstructure of nanocoating that induces a relatively high incidence of the lubricating oxide films [7]. It can be observed from Fig. 4(e) that no extensive cracks appear on the worn surface of nanostructured coating. Moreover, pull-out of carbide particle and fatigue delamination (region marked by ellipse) are observed on conventional coating besides cracks (Fig. 4(b)), which give contribution to the overall wear rate. For both WC-CoCr coatings, the ductile Co-Cr matrix as preferential wear initiation site would undergo severe deformation at the beginning of the test, resulting in crack propagation prior to the occurrence of other wear mechanisms [40]. As the test continues, carbide particles are pulled out due to the disruption of carbide-binder interfaces, followed by fatigue delamination as a result of intensified plastic deformation for conventional coating. However, considerable amounts of oxide films and relatively higher  $H/E$  prevent nanostructured coating from sticking to the alumina counterpart, which can be the reason that the wear rate of nanostructured coating is lower than that of

conventional coating at 350 °C. Based on the above analysis, carbide particle pull-out following the crack propagation and fatigue delamination contribute to the sliding wear mechanism of conventional coating, while binder extrusion is the predominant wear mechanism for nanostructured coating at 350 °C.

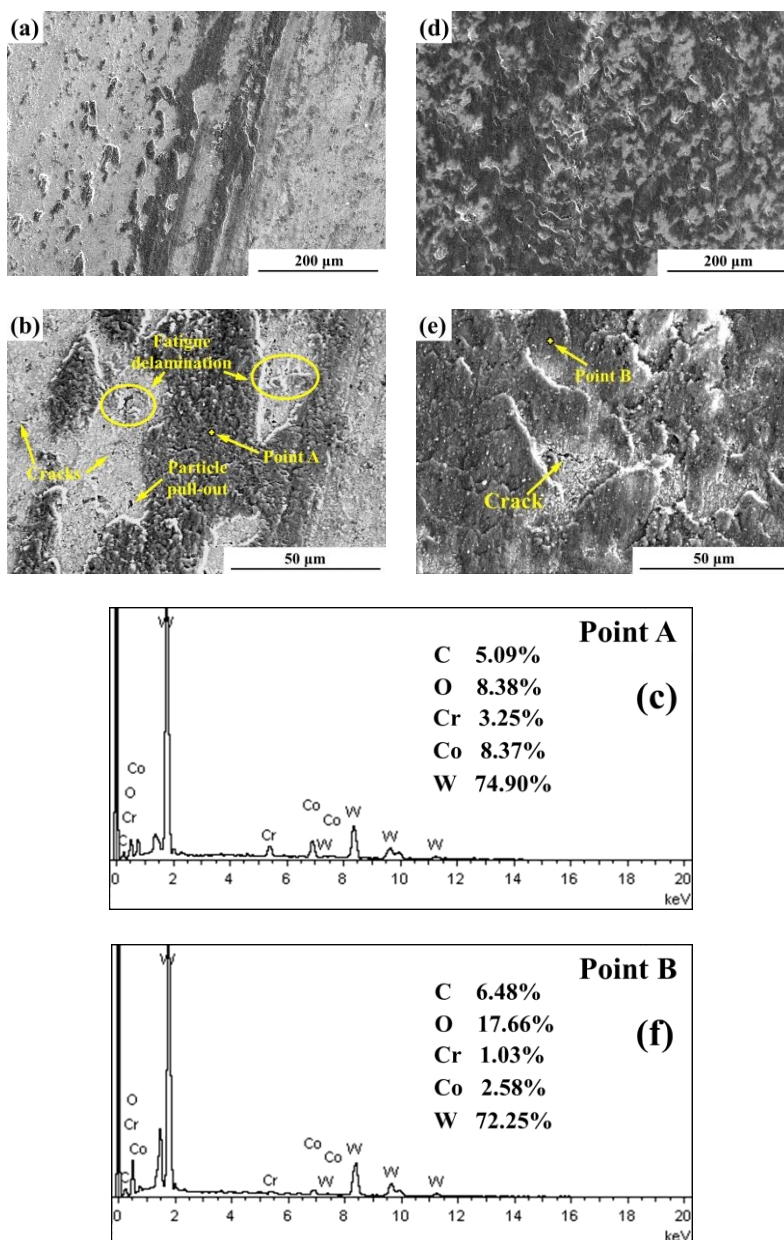


Fig. 4 SEM images and EDS analyses from worn surfaces of HVOF sprayed conventional (a-c) and nanostructured (d-f) WC-CoCr coatings

#### 4. Conclusions

Both conventional and nanostructured WC-CoCr coatings with low porosity were well-bonded to the substrates by HVOF spraying process. Nanostructured coating presented slightly lower hardness ( $H$ ) and elastic modulus ( $E$ ) and slightly higher ratios of  $H/E$  and  $H^3/E^2$ , as

compared to conventional coating. Nanostructured coating also exhibited higher wear resistance than its conventional counterpart in terms of lower friction coefficient, lower  $R_a$  value of worn surface and the absence of carbide particle pull-out and fatigue delamination. The superior sliding wear resistance of nanostructured coating was mainly attributed to its relatively higher  $H/E$  and considerable amounts of oxide films on the worn surface. In air at 350 °C, the main wear mechanism of conventional coating was carbide particle pull-out following the crack propagation and fatigue delamination, while binder extrusion was found to be the predominant sliding wear mechanism for nanostructured coating.

### Acknowledgments

The research was supported by the Natural Science Foundation of Jiangsu Province of China (Grant No. BK20150806), the China Postdoctoral Science Foundation (Grant No. 2016M590404), the National Natural Science Foundation of China (Grant Nos. 51609067, 51579087 and 51339005), and the Postdoctoral Science Foundation of Jiangsu Province of China (Grant No. 1601180C). The authors also gratefully acknowledge the financial support from the CAS Key Laboratory of Nuclear Materials and Safety Assessment, Institute of Metal Research, Chinese Academy of Sciences (Grant No. 2016NMSAKF03).

### References

- [1] R.J.K. Wood, *Int. J. Refract. Met. Hard Mater.* **28**, 82 (2010).
- [2] W. Tillmann, L. Hagen, D. Stangier, Iris-Aya Laemmerhirt, D. Biermann, P. Kersting, E. Krebs, *Surf. Coat. Technol.* **280**, 16 (2015).
- [3] A. Khosravifard, E. Salahinejad, A.H. Yaghtin, A. Araghi, A. Akhbarizadeh, *Ceram. Int.* **41**, 5713 (2015).
- [4] M.A. Zavareh, A.A.D.M. Sarhan, B.B. Razak, W.J. Basirun, *Ceram. Int.* **41**, 5387 (2015).
- [5] J.A. Picas, M. Punset, S. Menargues, E. Martín, M.T. Baile, *Surf. Coat. Technol.* **268**, 317 (2015).
- [6] P.H. Shipway, D.G. McCartney, T. Sudaprasert, *Wear* **259**, 820 (2005).
- [7] A. Lekatou, D. Sioulas, A.E. Karantzalis, D. Grimanelis, *Surf. Coat. Technol.* **276**, 539 (2015).
- [8] M. Kovaleva, Y. Tyurin, N. Vasilik, O. Kolisnichenko, M. Prozorova, M. Arsenko, M. Yapryntsev, V. Sirota, I. Pavlenko, *Ceram. Int.* **41**, 15067 (2015).
- [9] Z. Zhou, L. Wang, D.Y. He, F.C. Wang, Y.B. Liu, *J. Therm. Spray Technol.* **19**(1), 1287 (2010).
- [10] M. Amiriyan, H.D. Alamdari, C. Blais, S. Savoie, R. Schulz, M. Gariépy, *Wear* **342-343**, 154 (2015).
- [11] M. Amiriyan, C. Blais, S. Savoie, R. Schulz, M. Gariépy, H. Alamdari, *Materials* **9**, 117 (2016).
- [12] D.A. Stewart, P.H. Shipway, D.G. McCartney, *Wear* **225-229**, 789 (1999).
- [13] A. Mateen, G.C. Saha, T.I. Khan, F.A. Khalid, *Surf. Coat. Technol.* **206**, 1077 (2011).
- [14] G. Bolelli, L.-M. Berger, T. Börner, H. Koivuluoto, L. Lusvarghi, C. Lyphout, N. Markocsan, V. Matikainen, P. Nylén, P. Sassatelli, R. Trache, P. Vuoristo, *Surf. Coat. Technol.* **265**, 125 (2015).
- [15] G.L. Hou, Y.L. An, X.Q. Zhao, H.D. Zhou, J.M. Chen, *Acta Mater.* **95**, 164 (2015).
- [16] Q.Q. Yang, T. Senda, A. Ohmori, *Wear* **254**, 23 (2003).
- [17] J.M. Guilemany, S. Dosta, J.R. Miguel, *Surf. Coat. Technol.* **201**, 1180 (2006).
- [18] A.K. Basak, J.-P. Celis, M. Vardavoulias, P. Matteazzi, *Surf. Coat. Technol.*

- 206**, 3508 (2012).
- [19] Y.F. Qiao, Y.R. Liu, T.E. Fischer, *J. Therm. Spray Technol.* **10**(1), 118 (2001).
- [20] A.H. Dent, S. DePalo, S. Sampath, *J. Therm. Spray Technol.* **11**(4), 551 (2002).
- [21] J.A.R. Wesmann, N. Espallargas, *Tribol. Int.* **101**, 301 (2016).
- [22] Z. Geng, S. Li, D.L. Duan, Y. Liu, *Wear* **330-331**, 348 (2015).
- [23] J.F. Archard, *J. Appl. Phys.* **24**, 981 (1953).
- [24] J. Halling, *Thin Solid Films* **108**, 103 (1983).
- [25] J. Musil, F. Kunc, H. Zeman, H. Poláková, *Surf. Coat. Technol.* **154**, 304 (2002).
- [26] S. Hong, Y.P. Wu, B. Wang, Y.G. Zheng, W.W. Gao, G.Y. Li, *Mater. Des.* **55**, 286 (2014).
- [27] S. Hong, Y.P. Wu, Y.G. Zheng, B. Wang, W.W. Gao, J.R. Lin, *Surf. Coat. Technol.* **235**, 582 (2013).
- [28] S. Hong, Y.P. Wu, W.W. Gao, B. Wang, W.M. Guo, J.R. Lin, *Surf. Eng.* **30**(1), 53 (2014).
- [29] Y.P. Wu, B. Wang, S. Hong, J.F. Zhang, Y.J. Qin, G.Y. Li, *Trans. Indian Inst. Metals* **68**(4), 581 (2015).
- [30] W.C. Oliver, G.M. Pharr, *J. Mater. Res.* **19**(1), 3 (2004).
- [31] ASTM G99-05, Standard Test Method for Wear Testing with a Pin-on-Disk Apparatus, ASTM International, West Conshohocken, PA, (2010).
- [32] C.J. Li, Y.Y. Wang, G.J. Yang, A. Ohmori, K.A. Khor, *Mater. Sci. Tech.* **20**, 1087 (2004).
- [33] L.D. Zhao, M. Maurer, F. Fischer, R. Dicks, E. Lugscheider, *Wear* **257**, 41 (2004).
- [34] O. Maranhão, D. Rodrigues, M. Boccalini, Jr., A. Sinatora, *Surf. Coat. Technol.* **202**, 3494 (2008).
- [35] J.B. Cheng, X.B. Liang, B.S. Xu, *Surf. Coat. Technol.* **235**, 720 (2013).
- [36] R.S. Lima, J. Karthikeyan, C.M. Kay, J. Lindemann, C.C. Berndt, *Thin Solid Films* **416**, 129 (2002).
- [37] A. Leyland, A. Matthews, *Wear* **246**, 1 (2000).
- [38] M. Dao, L. Lu, R.J. Asaro, J.T.M. De Hosson, E. Ma, *Acta Mater.* **55**, 4041 (2007).
- [39] W. Tillmann, I. Baumann, P.S. Hollingsworth, L. Hagen, *J. Therm. Spray Technol.* **23**(1-2), 262 (2014).
- [40] M. Jafari, M.H. Enayati, M. Salehi, S.M. Nahvi, S.N. Hosseini, C.G. Park, *J. Therm. Spray Technol.* **23**(8), 1456 (2014).